frontiers

Supplementary Material

Contents

Text S1: Comparison of robust regression estimators for seismic array data processing.

Here, we compare the performance of a Biweight M-estimator, implemented via iteratively reweighted least squares (IRLS), and least trimmed squares (LTS) regression.

The least trimmed squares estimator is considered a high breakdown point estimator (*Bishop et al., 2020*), which is widely spread in modern literature (e.g., *Atkinson & Cheng, 1999; Mount et al., 2014*). It reduces influences from outliers by performing least squares fits over sub-samples of the original data set (*Rousseeuw, 1984; Rousseeuw & Leroy, 1987*):

$$\hat{\vec{\beta}} = \underset{\vec{\beta}}{argmin} \sum_{i=1}^{h \leq N} \left|\epsilon_i(\vec{\beta})\right|_i^2 \quad (1)$$

with h defining the size of the sub-sample, and ${\epsilon_1}^2 \leq {\epsilon_2}^2 \ldots \leq {\epsilon_N}^2$ are the numerically ascending squared residuals. One method to determine the sub-sample that minimizes the error function is given by the FAST-LTS algorithm (*Rousseeuw & Van Driessen, 1999 & 2006*, for details see also *Bishop et al., 2020*). The choice of the sub-sample size h, which is usually expressed as a fraction of the size of the whole data set (N), is a trade-off between a high breakdown point (small h) and statistical efficiency (large h) (*Rousseeuw & Hubert, 1997*).

Bishop et al. (*2020*) compare the performance of weighted M-estimaton and least trimmed squares regression (LTS) for synthetical and observed infrasound data. They conclude that for the artificial examples both estimators perform well, whilst for real data LTS outperforms IRLS. We test both approaches for an exemplary event from the Insheim reservoir (M_L 0.5, BAZ to network localization: 97,5°), with the IRLS estimator implemented as described in *Holland and Welsch* (*1977*) and *Du Mouchel and O'Brien* (*1989*) and weights calculated according to equations (16.1) and (16.2) (see main manuscript). The FAST-LTS algorithm is provided through the MATLAB FSDA toolbox (*Riani et al., 2012*, following *Rousseeuw & Van Driessen, 2006*).

Figure S1B shows results for back azimuth (BAZ) and horizontal apparent velocity ($v_{app,h}$) for the exemplary event, with correlation windows shifted in 0.1 s steps relative to the point of maximum correlation ($argmax(MC)$). The left and right columns compare between a moderate (tc: 4.65; h: 0.75) and strong tuning (tc: 3; h: 0.5) of the robust estimators, respectively. Results from an ordinary least squares regression (OLS) are included for comparison. It shows that the results are always unstable for a negative shift, since in this case the correlation window does not include enough signal components (cf. Fig. 3B, main manuscript). The IRLS estimator (tc: 4.65 and 3) yields stable estimates for positive values, almost to the maximum shift of 1.5 s. The back azimuth lies within the 97.5° ± 2.5° range related to the network localization and the horizontal apparent velocity is approximately 7 km/s. OLS results are comparable to IRLS in the shift interval from 0 to 0.4 s, but they become unstable for larger shift values. Looking at the LTS estimator with a default sub-sample size (h: 0.75) reveals back azimuth values that are slightly smaller and less stable, but overall similar to IRLS. For the smaller sub-sample size (h: 0.5), the back azimuth values are systematically too small with reference to the network localization. The horizontal apparent velocity takes consistent values around 6 km/s.

Figure S1C examines the differences between the regression approaches through partial regression leverage plots for the first predictor variable ($\vec{x}$) and a correlation window at $argmax(MC) + 0.9\ s$. The associated delay times include two distinct outliers, making the OLS result unreliable. More interestingly, the LTS estimator extracts a sub-sample, which has a different slope than the bulk of the data. The sub-sample includes delay times related to the six inner array stations and excludes the outer sites (ST6, ST7, ST9 and ST10, cf. Figure 2, main manuscript). In contrast, the IRLS estimator removes

the influence of the two outliers, but the parameter estimate is still determined by the bulk of the data. Figure 5D visualizes the estimated BAZ and $v_{app,h}$ values for OLS, IRLS and LTS regression in a polar diagram plot.

The IRLS estimator performs equally well for larger numbers of outliers. Fig. S2 shows an example for the same event as in S1 but with the correlation window at $argmax(MC) + 1.4\ s$ (~25% outliers for the delay times). If the proportion of outliers approaches 50%, e.g., when the correlation window includes only P-wave coda, the LTS estimator is superior. However, this is not the regular case and a successful implementation in an automatized real-time application would require prior knowledge regarding the number of outliers.

Bishop et al. (*2020*) state that weighted M-estimation does not significantly improve their infrasound processing if applied to real data. Our results for seismic array data do not support this conclusion. The IRLS estimator, in combination with the Biweight function from equation (16) (main manuscript), yields stable and consistent results for BAZ and apparent velocity, even in the presence of corrupted data. Iteratively reweighted least squares proves to be particularly well suited, as it diminishes effects from outliers by dragging them towards a normal distribution, whilst the parameter estimates are defined by the mean of the data. LTS, on the other hand, is a highly robust sub-set algorithm, but it is to be handled with caution for data sets that include slightly differing data populations (see Víšek, 2000 for a detailed discussion). In our case, the LTS algorithm neglects observations from the outer array sites, which are crucial for the accuracy of the localization. Excluding individual sites from the analysis changes the array geometry and consequently the array transfer function, which is usually optimized for slowness estimates in a specific frequency range (see *Harjes and Henger, 1973*; *Johnson and Dudgeon 1993* or *Schweizer et al., 2002*). Based on these results we decide to use the IRLS algorithm for our analysis.

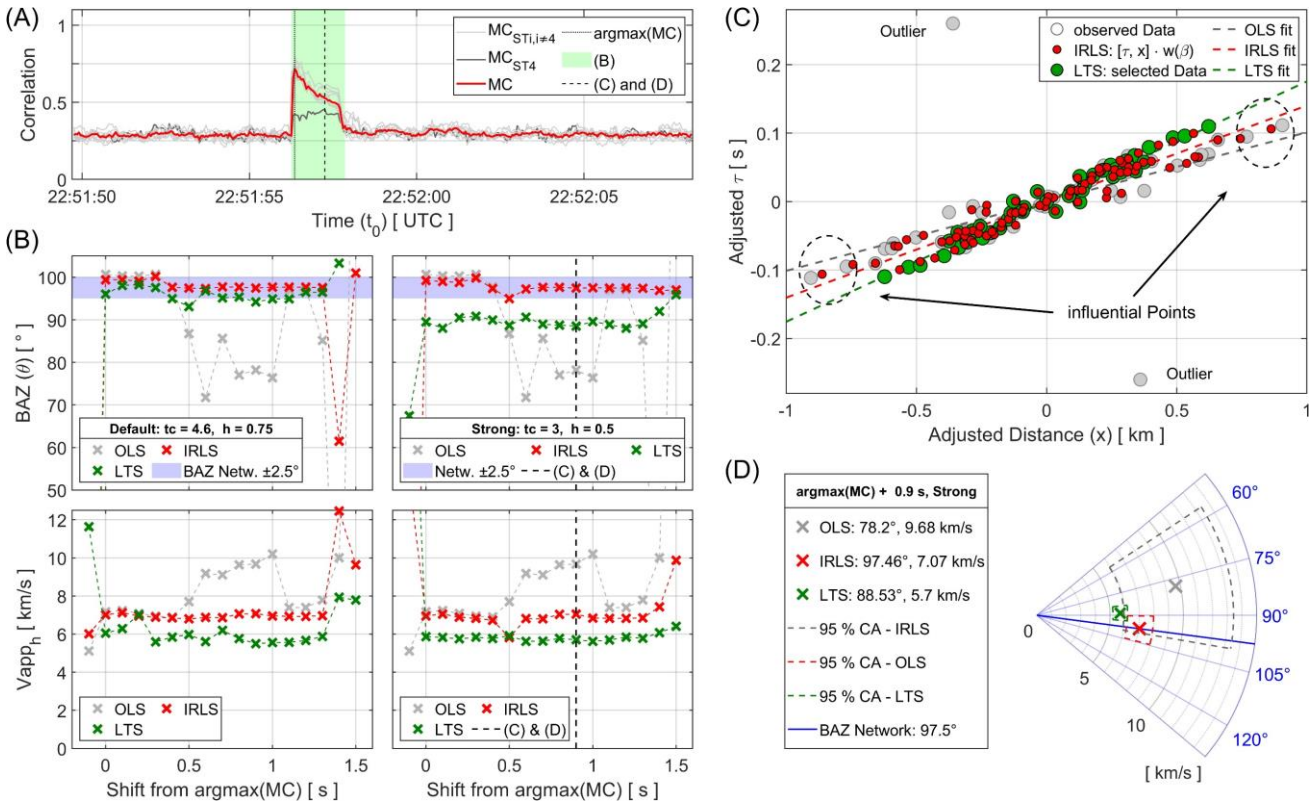

Figure S1: Comparison between IRLS and LTS regression for an exemplary event from the Insheim reservoir (M_L 0.5, BAZ 97,5°). Results for two significant outliers (see C and D). (A) Median of the cross-correlation matrix (MC) for all sites (red line) and for the individual sites (grey lines). The correlation for site ST4 (black line) is attenuated, which relates to a worse self-noise of the short period instrument. The dotted black line indicates the point of maximum correlation ($argmax(MC)$). The green area shows the positions of the 1.5 s long correlation windows used in B, the dashed black line the position in C and D. (B) Results for BAZ and $v_{app,h}$ in dependence of the shift relative to the point of maximum correlation for the IRLS, LTS and OLS estimators. The left and right columns compare between a moderate (tc: 4.65; h: 0.75) and strong tuning (tc: 3; h: 0.5) of the robust estimators, respectively. The back azimuth of the network localization is indicated by the blue area (97.5° ± 2.5°) (C) Partial regression leverage plots for the first predictor variable ($\vec{x}$) at $argmax(MC) + 0.9\ s$. The large circles show the adjusted time delays for the OLS regression, including two distinct outliers. Circles in green mark observations selected by the LTS algorithm. The selected subset omits observations from the outer array sites, including the influential (high leverage) points at the boundaries, resulting in a biased slope of the LTS regression. The IRLS algorithm (small red circles) drags outliers toward a normal distribution, but the regression result is determined by the bulk of the data. (D) Results from the IRLS, LTS and OLS estimators at $argmax(MC) + 0.9\ s$. The dashed lines enclose the 95% confidence areas (CA).

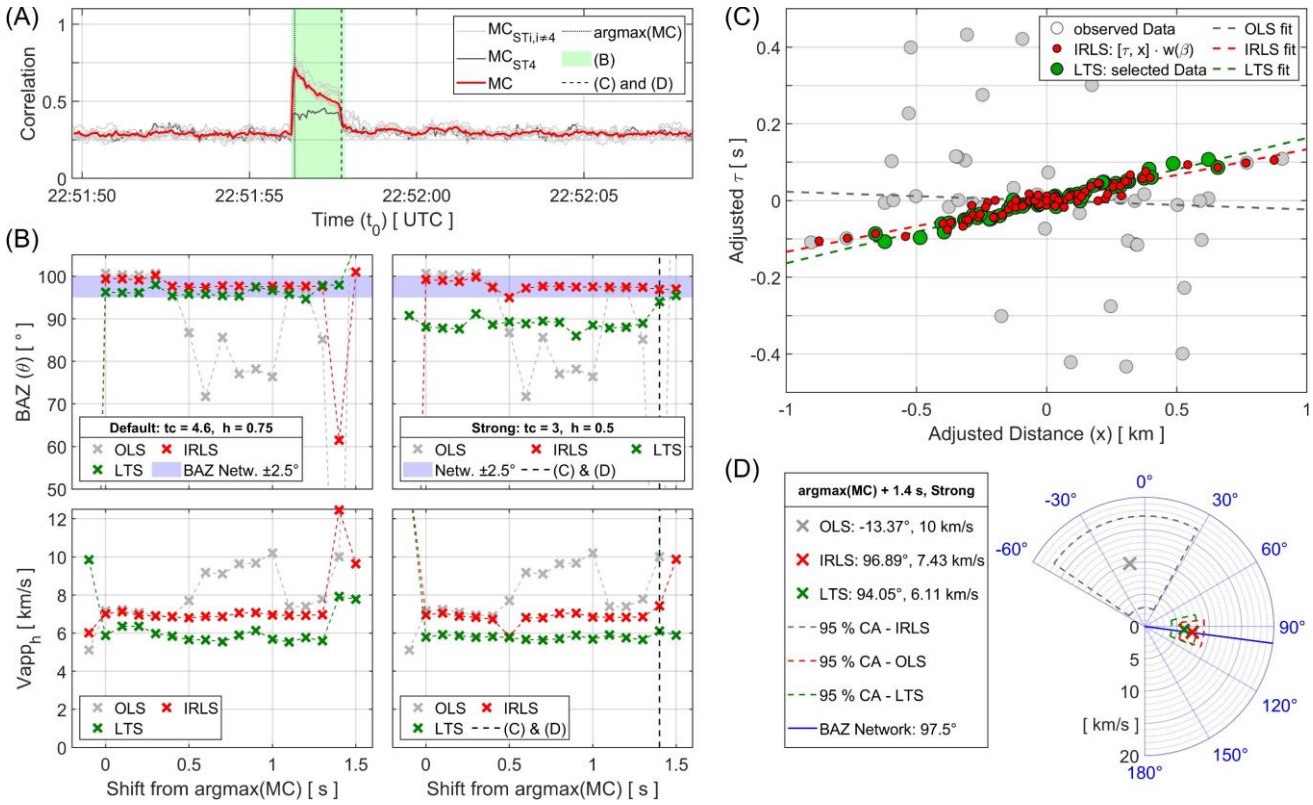

Figure S2: Comparison between IRLS and LTS regression for an exemplary event from the Insheim reservoir (M_L 0.5, BAZ 97,5°). Results for multiple (~ 25 %) outliers (see C and D). (A) Median of the cross-correlation matrix (MC) for all sites (red line) and for the individual sites (grey lines). The correlation for site ST4 (black line) is attenuated, which relates to a worse self-noise of the short period instrument. The dotted black line indicates the point of maximum correlation ($argmax(MC)$). The green area shows the positions of the 1.5 s long correlation windows used in B, the dashed black line the position in C and D. (B) Results for BAZ and $v_{app,h}$ in dependence of the shift relative to the point of maximum correlation for the IRLS, LTS and OLS estimators. The left and right columns compare between a moderate (tc: 4.65; h: 0.75) and strong tuning (tc: 3; h: 0.5) of the robust estimators, respectively. The back azimuth of the network localization is indicated by the blue area (97.5° ± 2.5°) (C) Partial regression leverage plots for the first predictor variable ($\vec{x}$) at $argmax(MC) + 1.4\ s$. The large circles show the adjusted time delays for the OLS regression, including two distinct outliers. Circles in green mark observations selected by the LTS algorithm. The selected subset omits observations from the outer array sites, including the influential (high leverage) points at the boundaries, resulting in a biased slope of the LTS regression. The IRLS algorithm (small red circles) drags outliers toward a normal distribution, but the regression result is determined by the bulk of the data. (D) Results from the IRLS, LTS and OLS estimators at $argmax(MC) + 1.4\ s$. The dashed lines enclose the 95% confidence areas (CA).

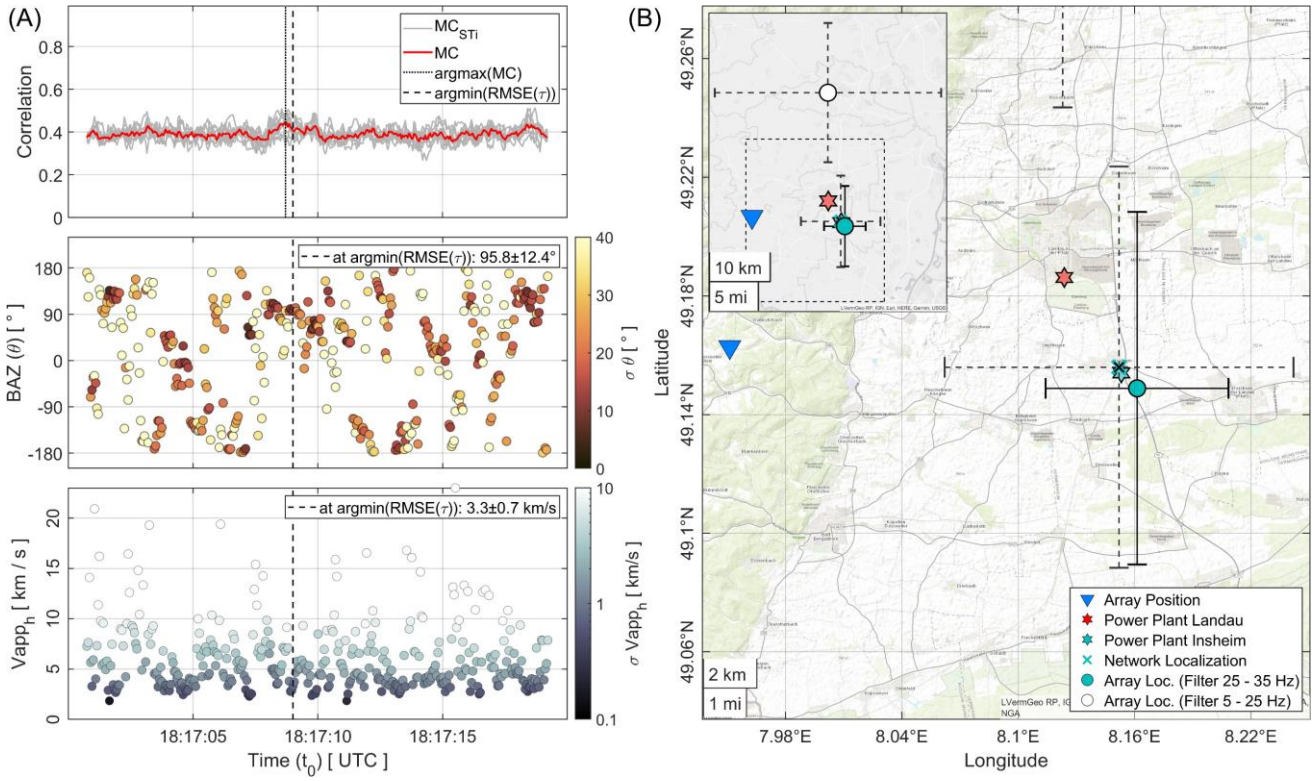

Figure S3: Re-evaluation of a low-quality localization (event from December 15, 2021, M_L 0.7) using an adapted bandpass filter between 25 and 35 Hz. (A) Top: Median of the cross-correlation matrix (MC) for all sites (red line) and for the individual sites (grey lines). The correlation function (MC) is not pronounced at the event. Center & Bottom: Time dependent back azimuth (BAZ) and horizontal apparent velocity ($v_{app,h}$). The solution for both parameters is not very stable during the event. However, the estimated BAZ of 95.8°, derived for the time window that minimizes the $RMSE$ of the linear regression, is adequate. (B) Map plot of the network (cyan cross) and array localization (cyan filled circle; bandpass filter between 25 and 35 Hz). The distance between both localizations is 1.2 km. The 95% confidence intervals for both methods are significant. The small map in the upper left compares the results to the original localization (white filled circle; bandpass filter between 5 and 25 Hz). The improvement is remarkable.

Table 1: Results for the array analysis. Columns indicated by (N) refer to information from the network catalogue (*LGB-RLP, 2022*). The exemplary event is highlighted in green. *SE* implies the standard error (σ).

Reservoir	*Source TIME*	*BAZ*	*SE BAZ*	*Vapp$_h$*	*SE Vapp$_h$*	*Vapp$_Z$*	*SE Vapp$_Z$*	*Distance*	*SE Distance*	*RMSE*
(N)	*(UTC) (N)*	*[°]*	*[°]*	*[km/s]*	*[km/s]*	*[km/s]*	*[km/s]*	*[km]*	*[km]*	*[s]*
Insheim	12.07.2021 16:42	99,1	4,7	6,2	0,6	3,2	1,8	14,53	1,23	0,049
Insheim	30.07.2021 19:46	101,5	1,7	6,2	0,2	5,9	2,2	13,76	0,77	0,018
Insheim	05.08.2021 23:33	107,5	3,3	5,8	0,4	8,3	7,7	14,23	0,81	0,03
Insheim	18.08.2021 06:18	108	1,8	5,5	0,2	26,4	40,3	14,53	0,82	0,016
Insheim	21.08.2021 16:25	103,9	2,4	6,4	0,3	11,2	10,4	14,58	0,82	0,024
Insheim	21.08.2021 16:26	98	8,1	7,1	1,2	12,4	38,4	14,09	0,94	0,072
Insheim	21.08.2021 17:00	103,4	2,5	6,3	0,3	13,3	13,7	14,51	0,81	0,024
Insheim	21.08.2021 17:18	104,2	2,4	6,5	0,3	15,1	18,9	14,29	0,8	0,024
Landau	13.09.2021 00:10	93,2	2,3	6,6	0,3	12,7	22,3	12,59	0,71	0,022
Landau	20.09.2021 00:34	80,4	1,1	5,7	0,1	3	0,4	12,68	0,72	0,012
Insheim	29.09.2021 12:09	100,1	2,6	6,9	0,4	4,2	1,6	14,23	0,8	0,024
Insheim	30.09.2021 23:15	98,9	2,2	7	0,3	5,8	2,3	14,17	0,79	0,02
Insheim	30.09.2021 23:15	100,8	2,2	7,3	0,3	6,5	2,8	14,2	0,79	0,019
Landau	06.10.2021 18:38	73	5,7	6,8	0,9	3,3	2,1	12,67	0,71	0,054
Landau	06.10.2021 18:39	72,7	2,2	6,8	0,3	4	1,2	12,37	0,7	0,021
Landau	06.10.2021 18:39	72,4	2,2	7	0,3	9,3	6	12,44	0,69	0,02
Insheim	03.11.2021 20:40	103,5	2,1	7,3	0,3	4,7	1,4	14,05	0,79	0,018
Landau	03.11.2021 22:17	72,2	4,3	7	0,7	4,5	2,6	12,49	0,7	0,039
Landau	03.11.2021 22:17	79,9	8,9	7,8	1,5	8,1	22,7	12,57	0,71	0,074
Landau	03.11.2021 22:18	71,3	2	6,7	0,3	5,8	2,3	12,67	0,71	0,02
Landau	03.11.2021 22:19	69,3	0,9	7	0,1	5,9	1,1	12,41	0,7	0,008
Landau	03.11.2021 22:20	71,2	2	6,7	0,3	4,2	1,2	12,52	0,71	0,019
Landau	03.11.2021 22:21	73,5	2,9	6,6	0,4	4,2	1,7	12,33	0,7	0,028
Landau	03.11.2021 22:22	72,8	3,7	6,5	0,5	3,3	1,4	12,44	0,7	0,037
Landau	03.11.2021 22:25	71,4	2,2	7	0,4	4,9	1,7	12,34	0,7	0,021
Landau	03.11.2021 22:26	65,8	1,6	5,4	0,2	4,5	1,5	12,29	0,69	0,018
Landau	03.11.2021 22:27	72,3	3,8	6,6	0,6	5,6	4	12,6	0,7	0,037
Landau	03.11.2021 22:28	74,3	1,9	6,4	0,3	3,9	1	12,61	0,7	0,019
Landau	03.11.2021 22:28	72,2	2,3	6,8	0,4	5,1	1,9	12,4	0,7	0,021
Landau	03.11.2021 22:29	73,8	1,9	6,6	0,3	4,9	1,6	12,34	0,69	0,019
Landau	03.11.2021 22:30	74	2	6,5	0,3	4,1	1,1	12,57	0,7	0,019
Landau	03.11.2021 22:30	74,1	3,3	6,6	0,5	4,5	2,2	12,64	0,71	0,032
Landau	03.11.2021 22:30	73,5	1,7	6,5	0,2	3,8	0,8	12,78	0,72	0,017
Landau	03.11.2021 22:31	71,8	1,9	6,6	0,3	4,4	1,2	12,23	0,69	0,018
Landau	03.11.2021 22:31	72	2,3	7	0,4	5,1	1,9	12,63	0,71	0,021
Landau	03.11.2021 22:32	74	2,7	6,2	0,4	5,2	2,5	12,52	0,7	0,028
Landau	03.11.2021 22:33	74,6	4,2	6,4	0,6	3,3	1,5	12,59	0,71	0,041
Landau	03.11.2021 22:46	72,2	1,9	6,6	0,3	4,3	1,2	12,53	0,7	0,019
Landau	30.11.2021 22:49	101,9	14,2	4,4	1,1	1,8	2,2	13,69	4,38	0,21
Landau	30.11.2021 22:49	68,5	25,7	6	2,8	0,5	0,3	20,54	2,33	0,274
Landau	03.11.2021 23:41	72,3	2,5	6,7	0,4	5,7	2,7	12,36	0,69	0,024
Landau	08.11.2021 02:05	41,9	4,1	5,7	0,6	5,1	4	12,62	0,72	0,046
Landau	08.11.2021 02:06	79,6	5,4	5,4	0,6	3,4	2,6	12,5	0,77	0,065
Landau	09.11.2021 02:40	73,5	3,1	5,8	0,4	2,9	1	12,78	0,72	0,035
Insheim	18.11.2021 06:58	96,8	3,5	6,8	0,5	2,9	0,9	13,88	0,78	0,033
Insheim	**19.11.2021 22:51**	**99,5**	**1,8**	**7,1**	**0,3**	**3,1**	**0,5**	**14,11**	**0,79**	**0,016**
Insheim	25.11.2021 00:08	97,9	2,5	6,9	0,3	3	0,7	14,06	0,79	0,023
Insheim	25.11.2021 02:12	100,3	5,6	7,3	0,9	5	4,7	14,1	0,79	0,05
Insheim	06.12.2021 16:50	97,1	7,1	6,8	1	3,3	2,5	14,31	0,8	0,068
Insheim	11.12.2021 04:13	99,9	5,4	6,9	0,8	3	1,5	13,96	0,78	0,05

Insheim	13.12.2021 21:01	98,6	5,8	7,3	0,8	5,8	6	14,18	0,8	0,049
Insheim	15.12.2021 18:17	31,4	52,1	11,3	10	0,4	0,1	23,64	3,96	0,291
Insheim	15.12.2021 23:02	96,4	4,4	7,3	0,6	3,1	1,3	14,81	0,83	0,039
Insheim	22.12.2021 01:21	170,4	31,7	9,2	4,9	0,5	0,1	11,78	2,04	0,216
Insheim	23.12.2021 13:54	50,3	38,5	8,4	5,7	1,3	1,4	8,52	1,4	0,293
Insheim	24.12.2021 20:18	69,8	22,2	5,2	2,1	0,9	0,7	17,33	4,13	0,278
Insheim	30.12.2021 18:31	23,5	56,3	15,1	10	1	0,4	12,45	3,38	0,234
Insheim	02.01.2022 23:04	163	33,2	6,6	3	0,6	0,2	22,98	0,29	0,228
Insheim	04.01.2022 04:16	104,2	4,5	7,1	0,7	2,8	1,1	13,9	0,78	0,04
Insheim	04.01.2022 16:52	104,5	3,4	7,2	0,5	3,1	1	14,22	0,91	0,03
Insheim	08.01.2022 07:28	101,8	2,6	6,3	0,4	3,9	1,4	13,51	0,76	0,027
Insheim	11.01.2022 21:38	102,3	4,3	6,3	0,6	5	3,7	14,3	0,81	0,043
Insheim	11.01.2022 22:36	176,2	46,5	10,7	8,3	0,6	0,3	10,63	2,24	0,272
Insheim	23.01.2022 12:31	116	3,7	6,9	0,6	3,7	1,7	22,77	1,28	0,031
Insheim	25.01.2022 15:27	102,6	4,3	6,2	0,5	4,1	2,6	14,14	0,79	0,039
Insheim	31.01.2022 04:06	101	4,4	6,2	0,6	3,6	2,1	14,26	0,82	0,041
Insheim	01.02.2022 00:48	100	1,4	6,2	0,2	3,4	0,6	14,01	0,78	0,012
Insheim	04.02.2022 18:49	172,1	64,4	14,9	4,9	0,4	0,1	10,91	3,41	0,254
Insheim	28.02.2022 19:32	100	1,1	6,2	0,1	3,7	0,6	13,98	0,78	0,01
Insheim	01.03.2022 22:39	101,8	1,7	6,2	0,2	3,5	0,8	14,46	0,81	0,016
Insheim	07.03.2022 03:05	97,9	1,7	6,2	0,2	3,9	0,9	14,51	0,81	0,016
Insheim	13.03.2022 00:42	100,6	3,3	6,1	0,4	4,2	2,2	14,09	0,79	0,031
Insheim	13.03.2022 01:54	100,3	4,1	6,2	0,5	4,5	1,6	14,2	0,79	0,037
Insheim	16.03.2022 01:11	99,4	1,5	6,2	0,2	4	0,9	14,23	0,8	0,014
Insheim	16.03.2022 14:53	99,8	1,5	6,2	0,2	4	0,9	14,14	0,79	0,013
Insheim	25.04.2022 00:58	96,6	8,2	8,2	1,2	20	30,5	14,19	0,06	0,065
Insheim	27.04.2022 22:54	98,6	1,8	6,4	0,2	16,4	16,5	14,64	0,82	0,018

Table 2: Results and comparison for array and network localizations. Columns indicated by (N) refer to the network catalogue (*LGB-RLP, 2022*), columns indicated by (A) to array localizations. The exemplary event is highlighted in green. The standard errors for Longitude and Latitude are derived as σd_x and σd_y (eq. 25 in the main manuscript). The last column includes the distance between array and network localizations. The array localizations are corrected for the systematical misfit in back azimuth (Insheim +4.1°, Landau -4.7°).

Reservoir	*Date*	*Mag.*	*Long.*	*SE Lon.*	*Lat.*	*SE Lat.*	*Long.*	*SE Lon.*	*Lat.*	*SE Lat.*	*Distance*
(N)	*(N)*	*(N)*	*(A)*	*(A)*	*(A)*	*(A)*	*(N)*	*(N)*	*(N)*	*(N)*	*(N - A)*
		M_L	*[°]*	*[km]*	*[°]*	*[km]*	*[°]*	*[km]*	*[°]*	*[km]*	*[km]*
Insheim	12.07.2021	0,9	8,15	1,23	49,152	1,19	8,178	11,77	49,095	11,82	6,62
Insheim	30.07.2021	0,7	8,139	0,77	49,147	0,42	8,148	2,24	49,153	1,83	0,93
Insheim	05.08.2021	0,4	8,142	0,81	49,133	0,82	8,22	4,77	49,184	4,44	8
Insheim	18.08.2021	1,2	8,145	0,8	49,132	0,49	8,164	1,74	49,185	1,67	6,08
Insheim	21.08.2021	1,1	8,149	0,81	49,141	0,62	8,146	1,46	49,149	1,56	0,94
Insheim	21.08.2021	0,5	8,145	0,95	49,154	1,99	8,16	2,22	49,162	2,46	1,4
Insheim	21.08.2021	1,2	8,148	0,81	49,142	0,64	8,146	1,54	49,149	1,64	0,8
Insheim	21.08.2021	0,8	8,145	0,79	49,141	0,61	8,151	1,67	49,154	2,24	1,57
Landau	13.09.2021	0,1	8,123	0,71	49,148	0,5	8,116	1,9	49,182	2,25	3,83
Landau	20.09.2021	0,5	8,125	0,72	49,173	0,24	8,118	3,13	49,185	3,13	1,41
Insheim	29.09.2021	1	8,146	0,8	49,15	0,64	8,144	2,7	49,138	2,93	1,31
Insheim	30.09.2021	0,5	8,145	0,79	49,152	0,54	8,156	1,61	49,153	1,39	0,77
Insheim	30.09.2021	0,3	8,145	0,79	49,148	0,54	8,162	1,76	49,161	1,77	1,88
Landau	06.10.2021	0,3	8,121	0,75	49,188	1,24	8,134	2,62	49,18	2,01	1,25
Landau	06.10.2021	0,5	8,117	0,69	49,188	0,49	8,073	6,46	49,19	4,84	3,22
Landau	06.10.2021	0,4	8,118	0,68	49,188	0,5	8,121	2,76	49,197	3,16	0,98
Insheim	03.11.2021	0,9	8,142	0,78	49,142	0,52	8,147	1,4	49,15	1,33	0,92
Landau	03.11.2021	0,2	8,118	0,72	49,189	0,93	8,131	2,11	49,185	1,62	1,01
Landau	03.11.2021	0	8,123	0,73	49,174	1,95	8,129	2,17	49,184	4,91	1,18
Landau	03.11.2021	0,3	8,12	0,7	49,191	0,47	8,132	2,16	49,188	2,1	0,92
Landau	03.11.2021	0,5	8,115	0,67	49,194	0,27	8,113	1,73	49,189	1,53	0,6
Landau	03.11.2021	1,3	8,118	0,7	49,191	0,46	8,116	1,06	49,192	1,03	0,2
Landau	03.11.2021	0	8,117	0,7	49,186	0,63	8,13	3,21	49,184	4,73	0,96
Landau	03.11.2021	-0,2	8,118	0,71	49,188	0,8	8,13	2,64	49,183	2,7	1
Landau	03.11.2021	0,6	8,116	0,69	49,19	0,5	8,12	1,86	49,188	1,65	0,38
Landau	03.11.2021	0,5	8,11	0,66	49,2	0,39	8,13	3,57	49,184	2,82	2,3
Landau	03.11.2021	0,4	8,12	0,71	49,189	0,83	8,132	3,93	49,184	2,68	1,03
Landau	03.11.2021	0,3	8,121	0,69	49,185	0,43	8,112	1,98	49,19	1,87	0,88
Landau	03.11.2021	0,7	8,117	0,69	49,189	0,51	8,115	1,44	49,191	1,27	0,31
Landau	03.11.2021	0,3	8,117	0,68	49,186	0,43	8,122	2,78	49,184	2,34	0,37
Landau	03.11.2021	0,2	8,121	0,69	49,186	0,44	8,113	1,68	49,189	1,94	0,68
Landau	03.11.2021	0,2	8,122	0,71	49,186	0,73	8,116	1,55	49,186	1,7	0,42
Landau	03.11.2021	1	8,123	0,71	49,187	0,4	8,12	1,29	49,191	1,17	0,51
Landau	03.11.2021	0,4	8,115	0,68	49,189	0,42	8,118	1,85	49,183	1,62	0,72
Landau	03.11.2021	0,2	8,12	0,7	49,19	0,52	8,123	2	49,184	1,73	0,65
Landau	03.11.2021	0,1	8,12	0,7	49,185	0,6	8,122	2,11	49,182	1,77	0,41
Landau	03.11.2021	-0,2	8,121	0,72	49,184	0,92	8,13	3,19	49,191	2,97	0,96
Landau	03.11.2021	0,7	8,119	0,69	49,189	0,44	8,118	1,24	49,19	1,11	0,14
Landau	30.11.2021	-0,1	8,132	4,31	49,128	3,48	8,114	3,86	49,189	2,68	6,88
Landau	30.11.2021	0,1	8,222	3,51	49,217	8,83	8,134	4,4	49,198	6,3	6,7
Landau	03.11.2021	0,3	8,117	0,68	49,188	0,55	8,121	1,68	49,182	1,68	0,78
Landau	08.11.2021	0	8,077	0,82	49,241	0,83	8,138	4,17	49,205	7,28	6
Landau	08.11.2021	0	8,122	0,78	49,175	1,17	8,134	4,4	49,202	7,28	3,16
Landau	09.11.2021	0,5	8,123	0,72	49,187	0,7	8,126	1,7	49,193	2,47	0,7
Insheim	18.11.2021	0,5	8,142	0,78	49,157	0,84	8,155	1,89	49,147	1,6	1,48
Insheim	**19.11.2021**	**0,5**	**8,144**	**0,79**	**49,151**	**0,44**	**8,149**	**2**	**49,148**	**1,86**	**0,5**

Insheim	25.11.2021	0,4	8,144	0,79	49,155	0,6	8,155	1,51	49,15	1,47	0,94
Insheim	25.11.2021	0,2	8,144	0,8	49,149	1,38	8,149	1,46	49,146	1,53	0,52
Insheim	06.12.2021	0,9	8,148	0,8	49,156	1,77	8,155	2,25	49,151	2,2	0,79
Insheim	11.12.2021	0,6	8,142	0,79	49,15	1,3	8,147	1,47	49,148	1,53	0,43
Insheim	13.12.2021	0,6	8,146	0,81	49,153	1,43	8,147	4,54	49,139	3,55	1,57
Insheim	15.12.2021	0,3	8,1	19,21	49,352	10,44	8,152	2,76	49,156	3,27	22,11
Insheim	15.12.2021	0,3	8,155	0,83	49,158	1,13	8,17	2,59	49,169	2,76	1,67
Insheim	22.12.2021	0,3	7,99	6,36	49,06	2,52	8,189	3,99	49,171	4,34	19,02
Insheim	23.12.2021	0,8	8,036	4,1	49,216	4,24	8,176	5,38	49,155	3,08	12,25
Insheim	24.12.2021	0,5	8,169	4,68	49,227	6,36	8,165	5,05	49,129	4,4	10,92
Insheim	30.12.2021	0,8	8,008	11,6	49,268	5,15	8,162	2,55	49,159	2,55	16,55
Insheim	02.01.2022	1	8,065	12,44	48,97	4,83	8,245	10,94	49,095	4,73	19,07
Insheim	04.01.2022	0,8	8,139	0,79	49,141	1,08	8,139	3,78	49,137	3,89	0,46
Insheim	04.01.2022	0,5	8,144	0,91	49,14	0,83	8,132	6,19	49,134	6,54	1,07
Insheim	08.01.2022	0,6	8,135	0,76	49,147	0,62	8,135	1,95	49,154	2,35	0,81
Insheim	11.01.2022	0,5	8,146	0,82	49,145	1,06	8,141	2,77	49,138	3,55	0,83
Insheim	11.01.2022	0,4	7,972	8,54	49,068	2,52	8,188	8,07	49,149	3,78	18,12
Insheim	23.01.2022	0,9	8,242	1,31	49,087	1,44	8,245	3,55	49,104	2,97	1,93
Insheim	25.01.2022	1,1	8,144	0,8	49,144	1,05	8,147	3,34	49,132	4,36	1,39
Insheim	31.01.2022	1,2	8,146	0,82	49,148	1,09	8,147	1,76	49,15	1,54	0,27
Insheim	01.02.2022	1,2	8,143	0,78	49,15	0,34	8,147	1,66	49,149	1,55	0,32
Insheim	04.02.2022	0,7	7,983	12,01	49,067	4,21	8,181	5,34	49,146	3,85	16,89
Insheim	28.02.2022	0,6	8,143	0,78	49,15	0,28	8,139	1,89	49,145	1,73	0,62
Insheim	01.03.2022	0,4	8,148	0,8	49,146	0,44	8,155	2,29	49,147	1,92	0,51
Insheim	07.03.2022	0,7	8,15	0,81	49,154	0,44	8,15	1,4	49,155	1,26	0,07
Insheim	13.03.2022	0,7	8,144	0,79	49,149	0,82	8,143	2,64	49,142	2,7	0,75
Insheim	13.03.2022	0,4	8,145	0,79	49,149	1	8,143	1,89	49,145	1,98	0,5
Insheim	16.03.2022	0,3	8,146	0,8	49,151	0,39	8,144	1,69	49,153	1,47	0,25
Insheim	16.03.2022	1	8,145	0,79	49,15	0,36	8,147	1,51	49,149	1,67	0,23
Insheim	25.04.2022	0,5	8,146	0,1	49,157	2,02	8,16	2,29	49,145	1,68	1,71
Insheim	27.04.2022	0,5	8,152	0,82	49,153	0,46	8,158	2,13	49,154	1,51	0,46

References

Atkinson, A.C., and Cheng, T.C. (1999). Computing least trimmed squares regression with the forward search. Statistics and Computing, 9(4), 251-263.

Bishop, J.W., Fee, D., Szuberla, C.A. (2020). Improved infrasound array processing with robust estimators. Geophysical Journal International, 221(3), 2058–2074. https://doi.org/10.1093/gji/ggaa110

Dumouchel, W., and O'brien, F. (1989). Integrating a robust option into a multiple regression computing environment. In Computer science and statistics: Proceedings of the 21st symposium on the interface, 297–302. Alexandria: American Statistical Association.

Harjes, H. P., & Henger, M. (1973). Array-seismologie. *Zeitschrift für Geophysik*, *39*, 865-905.

Holland, P.W., and Welsch, R.E. (1977). Robust regression using iteratively reweighted least-squares. Communications in Statistics-theory and Methods, 6(9), 813-827. https://doi.org/10.1080/03610927708827533

Johnson, D. H., & Dudgeon, D. E. (1993). Array Signal Processing: Concepts and Techniques. Prentice Hall signal processing series, PTR Prentice-Hall. ISBN 0-13-048513-6.

Mount, D. M., Netanyahu, N. S., Piatko, C. D., Silverman, R., & Wu, A. Y. (2014). On the least trimmed squares estimator. Algorithmica, 69, 148-183. https://doi.org/10.1007/s00453-012-9721-8

Riani, M., Perrotta, D., & Torti, F. (2012). FSDA: A MATLAB toolbox for robust analysis and interactive data exploration. Chemometrics and Intelligent Laboratory Systems, 116, 17-32. https://doi.org/10.1016/j.chemolab.2012.03.017

Rousseeuw, P.J. (1984). Least median of squares regression. Journal of the American statistical association, 79(388), 871-880. 10.1080/01621459.1984.10477105

Rousseeuw, P.J., and Leroy, A.M. (1987). Robust Regression and Outlier Detection, John Wiley and Sons, Inc.

Rousseeuw, P. J., & Hubert, M. (1997). Recent developments in PROGRESS. Lecture Notes-Monograph Series, 201-214. https://www.jstor.org/stable/4355978

Rousseeuw, P. J., & Van Driessen, K. (2006). Computing LTS regression for large data sets. Data mining and knowledge discovery, 12, 29-45. https://doi.org/10.1007/s10618-005-0024-4

Schweitzer, J., Fyen, J., Mykkeltveit, S., Gibbons, S. J., Pirli, M., Kühn, D., Kværna, T. (2012). Seismic arrays. In New manual of seismological observatory practice 2 (NMSOP-2) 1–80. Deutsches GeoForschungsZentrum GFZ. 10.2312/GFZ.NMSOP-2_ch9

Víšek, J. Á. (2000). On the diversity of estimates. Computational Statistics & Data Analysis, 34 (1), 67-89, ISSN 0167-9473. https://doi.org/10.1016/S0167-9473(99)00068-7